**Proceedings of ASME TURBO EXPO 2002**
**Amsterdam, The Netherlands, June 2002**

# GT-2002-30082

# HIGH POWER DENSITY SILICON COMBUSTION SYSTEMS FOR MICRO GAS TURBINE ENGINES

**C. M. Spadaccini, J. Lee,**
**S. Lukachko, I. A. Waitz**
Gas Turbine Laboratory
Dept. of Aeronautics and Astronautics
Massachusetts Institute of Technology
Cambridge, MA 02139

**A. Mehra**
D-STAR Engineering Corp.
Shelton, CT 06484

**X. Zhang**
Dept. of Manufacturing Engineering
and Fraunhofer USA Center for
Manufacturing Innovation
Boston University
Boston, MA 02115

## ABSTRACT

As part of an effort to develop a micro-scale gas turbine engine for power generation and micro-propulsion applications, this paper presents the design, fabrication, experimental testing, and modeling of the combustion system. Two radial inflow combustor designs were examined; a single-zone arrangement and a primary and dilution-zone configuration. Both combustors were micro-machined from silicon using Deep Reactive Ion Etching (DRIE) and aligned fusion wafer bonding. Hydrogen-air and hydrocarbon-air combustion was stabilized in both devices, each with chamber volumes of 191 $mm^3$. Exit gas temperatures as high as 1800 K and power densities in excess of 1100 $MW/m^3$ were achieved. For the same equivalence ratio and overall efficiency, the dual-zone combustor reached power densities nearly double that of the single-zone design. Because diagnostics in micro-scale devices are often highly intrusive, numerical simulations were used to gain insight into the fluid and combustion physics. Unlike large-scale combustors, the performance of the micro-combustors was found to be more severely limited by heat transfer and chemical kinetics constraints. Important design trades are identified and recommendations for micro-combustor design are presented.

## NOMENCLATURE

| | |
|---|---|
| A | Arrhenius pre-exponential factor |
| a,b | Arrhenius exponents |
| $d_h$ | hydraulic diameter |
| $Da_h$ | homogeneous Damköhler number |
| $E''$ | heat loss |
| E | heat generated |
| $E_a$ | activation energy |
| h | enthalpy |
| LHV | lower heating value |
| $\dot{m}$ | mass flow |
| P | pressure |
| $Q_{loss}$ | heat loss from combustor |
| R | gas constant |
| T | temperature |
| V | volume |
| $\eta_c$ | overall combustor efficiency |
| $\eta_{chemical}$ | chemical efficiency |
| $\eta_{thermal}$ | thermal efficiency |
| $\rho$ | fluid density |
| $\tau_{reaction}$ | reaction time |
| $\tau_{residence}$ | residence time |

### Subscripts

| | |
|---|---|
| a | air |
| f | fuel |
| 0 | initial condition |
| 1 | combustor inlet |
| 2 | combustor exit |

## 1.0 INTRODUCTION

Recent advances in silicon micro-fabrication techniques and microelectromechanical systems (MEMS) have led to the possibility of a new generation of micro heat engines for power generation and micro air-vehicle propulsion applications. Epstein *et al.* [1] and Groshenry [2] have reported the design for a silicon-based, micro gas turbine generator capable of producing 10-50 Watts of power in a volume less than 1 $cm^3$ while consuming 7 grams of fuel per hour. This represents a ten-fold increase in power density over the best available batteries. Like their larger counterparts, an engine of the type shown in Figure 1 requires a high temperature combustion system to convert chemical energy into fluid thermal and kinetic energy.

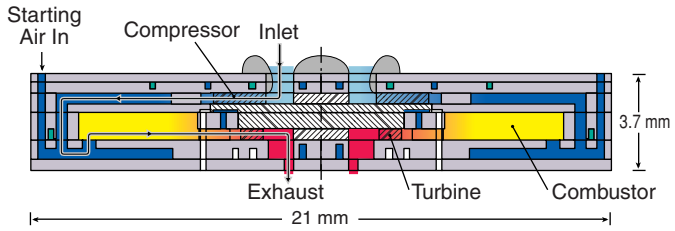


**Figure 1: Baseline engine schematic.**

This paper seeks to elucidate the underlying physics unique to micro-scale combustion systems through an experimental, computational, and analytical investigation. These studies have resulted in the identification of critical design trades and recommendations for micro-combustor design.

The work presented here is part of a broader effort to fabricate and operate this micro-scale gas turbine engine. The development strategy involves concurrently developing component technologies such as micro-compressors, gas bearings, and micro-combustors. All of these individual components have undergone independent testing and the first build of the engine has recently been completed.

The objective of a separate combustor test rig is to study combustor performance without the complexity of the full engine. The designs presented here retain most of the important functionality and boundary conditions of the engine. This includes overall flow-path and geometry, inlet swirl angle, combustor pressure, exit area, and back-pressure. The primary difference between the combustor rigs and the actual engine is the lack of a rotor. The tests are intended to explore the operating space of these combustors in an effort to determine if they provide adequate residence time, turbine inlet temperature, mass flow, and pressure ratio for the engine cycle. The final engine design will reflect these findings as well as those from other component experiments and analyses.

Section 2 discusses the challenges of combustion in a micro-scale environment and overviews previous work towards the development of silicon-based systems. The design and testing methodology for two micro-combustion devices are introduced in Section 3. In Section 4, results from the experiments are presented, complemented by results from computations and analysis. The results are synthesized in Section 5 as an operating space and in Section 6, the resulting design trades are reviewed. Section 7 summarizes and concludes the paper.

## 2.0 MICRO-COMBUSTION CHALLENGES

The functional requirements of a micro-combustor are similar to those of a conventional gas turbine combustor. These include the efficient conversion of chemical energy to fluid thermal and kinetic energy with low total pressure loss, reliable ignition, and wide flammability limits. However, the obstacles to satisfying these requirements are different for a micro-scale device. As first described by Waitz *et al*. [3] a micro-scale combustor is more highly constrained by inadequate residence time for complete combustion and high rates of heat transfer from the combustor. Micro-combustor development also faces unique challenges due to material and thermodynamic cycle constraints. These constraints are reviewed in the following sections.

### 2.1 Time-Scale Constraints

For the energy conversion applications we are interested in, power density is the most important metric. As shown in Table 1, the high power density of a micro-combustor directly results from high mass flow per unit volume. Since chemical reaction times do not scale with mass flow rate or combustor volume, the realization of this high power density is contingent upon completing the combustion process within a shorter combustor through-flow time.

**Table 1: A comparison of the operating parameters and requirements for a microengine combustor with those estimated for a conventional GE90 combustor.**

| | Conventional Combustor | Micro-Combustor |
|---|---|---|
| Length | 0.2 m | 0.001 m |
| Volume | 0.073 $m^3$ | $6.6\times10^{-8}$ $m^3$ |
| Cross-sectional area | 0.36 $m^2$ | $6\times10^{-5}$ $m^2$ |
| Inlet total pressure | 37.5 atm | 4 atm |
| Inlet total temperature | 870 K | 500 K |
| Mass flow rate | 140 kg/s | $1.8\times10^{-4}$ kg/s |
| Residence time | ~7 ms | ~0.5 ms |
| Efficiency | >99% | >90% |
| Pressure ratio | >0.95 | >0.95 |
| Exit temperature | 1800 K | 1600 K |
| Power Density | 1960 $MW/m^3$ | 3000 $MW/m^3$ |

*(Note: residence times are calculated using inlet pressure and an average flow temperature of 1000 K.)*

This fundamental time constraint can be quantified in terms of a homogeneous Damköhler number; the ratio of the residence time to the characteristic chemical reaction time.

$$Da_h = \frac{\tau_{residence}}{\tau_{reaction}} \tag{1}$$

To ensure a $Da_h$ greater than unity (and complete combustion), a designer of a micro-combustor can either increase the flow residence time or decrease the chemical reaction time. The characteristic combustor residence time is given by the bulk flow through the combustor volume.

$$\tau_{residence} \approx \frac{\text{volume}}{\text{volumetric flow rate}} = \frac{VP}{\dot{m}RT} \tag{2}$$

Residence time can be increased by increasing the size of the chamber, reducing the mass flow rate, or increasing the operat-

ing pressure. A chemical reaction time can be approximated by an Arrhenius type expression.

$$\tau_{reaction} \approx \frac{[fuel]_0}{A[fuel]^a[O_2]^b e^{-E_a/RT_0}} \quad (3)$$

Reaction time is primarily a function of fuel properties and the mixture temperature and pressure.

Since high power density requirements mandate high mass flow rates through small chamber volumes, the mass flow rate per unit volume can not be reduced without compromising device power density. Hence, there is a basic tradeoff between power density and flow residence time.

$$\text{Power density} \propto \frac{\dot{m}}{V} \propto \frac{\dot{m}_f LHV}{V} \propto \frac{\rho}{\tau_{residence}} \quad (4)$$

For a given operating pressure (and thus density), and assuming a $Da_h$ of unity, reducing the chemical reaction time and thus required residence time is the only means of ensuring complete combustion without compromising the high power density of the device.

Mixing time-scales are also critical in micro-combustion systems. Due to the small length-scales there is little time for fuel-air mixing and inadequate mixing can also lead to chemical inefficiency.

### 2.2 Heat Transfer Effects and Fluid-Structure Coupling

Energy loss due to heat transfer at the walls of the combustion chamber in a conventional gas turbine is typically neglected. However, for a micro-combustor this is an important factor. The surface-area-to-volume ratio for a micro-scale combustor is approximately 500 $m^{-1}$, or two orders of magnitude larger than that of a typical combustor.

Waitz *et al*. [3] have shown that the ratio of heat lost to that generated scales with the hydraulic diameter as follows:

$$\frac{E''}{\dot{E}} \propto \frac{1}{d_h^{1.2}} \quad (5)$$

The hydraulic diameter of a micro-combustor is on the order of millimeters, hundreds of times smaller than that of a typical combustor. Therefore, the ratio of heat lost to that generated may be as much as two orders of magnitude greater than that of a large-scale combustor.

The effects of this large surface heat loss on combustion are twofold. First, large thermal losses have a direct impact on overall combustor efficiency. Therefore, typical large-scale combustor efficiencies of greater than 99% are not feasible. Second, they can increase kinetic times and narrow flammability limits through lowering reaction temperatures. This can exacerbate the constraints of short residence time.

### 2.3 Recirculation Zones

Another important factor to consider in micro-combustor development is the design of recirculation zones for ignition and flame stability. To maintain high power density a flame-holding structure in a micro-combustion system must not only stabilize the flame, but must do it in a manner that efficiently uses the space within the combustor. Large recirculation zones or designs that do not initiate reactions rapidly in all portions of the flow reduce the power density that can be achieved in the device.

### 2.4 Material Constraints

There are also several material constraints imposed upon a silicon micro-combustion system. The most critical requirement is a wall temperature limit of less than 950 K. At temperatures above this level, silicon begins to soften and lose its structural integrity. However, high surface heat transfer and the high thermal conductivity of silicon are beneficial in this case. Combustor wall temperatures can be kept below the 950 K requirement by conduction of heat through the structure to the ambient. In addition, the rotating components of the micro-engine must maintain even lower wall temperatures, below 900 K, due to creep considerations.

### 2.5 Design Space

While time scale, heat transfer, and material constraints are important, the most limiting are those imposed by the engine thermodynamic cycle. Figure 2 shows a typical design space for a hydrogen-fueled micro-scale combustor. Equivalence ratio is plotted on the x-axis versus heat loss on the y-axis. A turbine inlet temperature between 1600 K and 1800 K is required for the cycle proposed for this engine. In Figure 2 the flame stability limit represents the stable operation of a non-adiabatic perfectly stirred reactor (PSR). The thermal stress constraint indicates the material limits of the all silicon structure of a micro-machined combustion system. The design space is further bounded by the desire to burn lean and the flammability limits of hydrogen-air combustion.

### 2.6 Previous Work

Mehra and Waitz [4] were the first to develop a silicon, micro-fabricated combustor compatible with a realistic engine

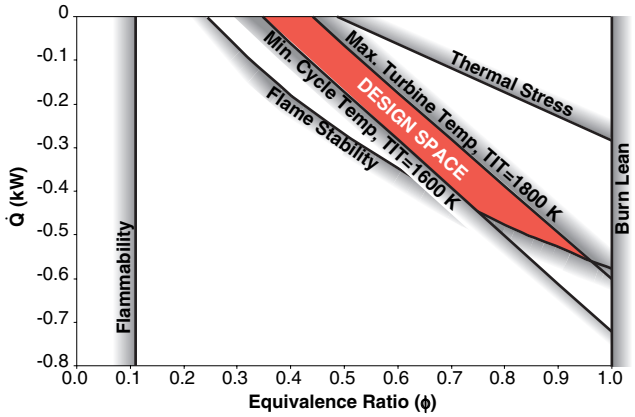


**Figure 2: Micro-combustor design space.**

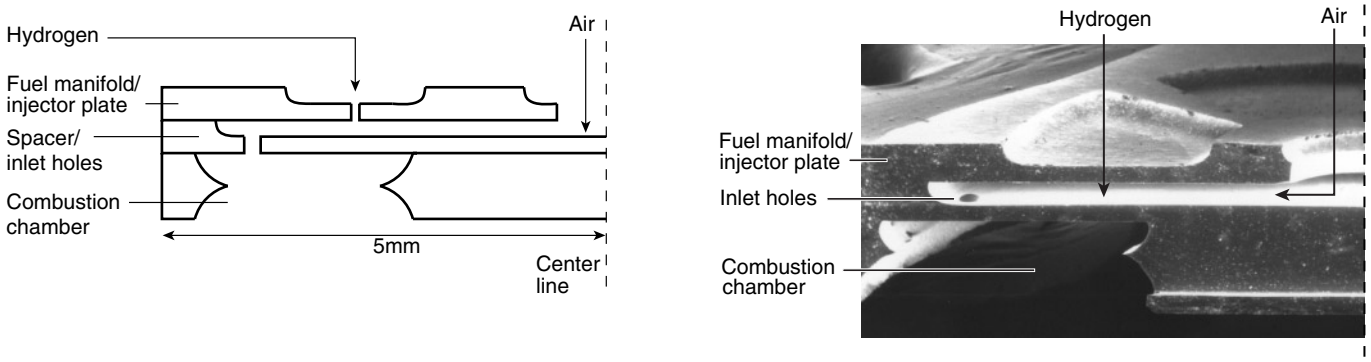


**Figure 3: Schematic and SEM of 0.066 cm$^3$ micro-combustor.**

geometry. This three-wafer combustor, shown in Figure 3, was 0.066 cm$^3$ in volume and was designed to operate using lean, premixed, hydrogen-air combustion. The device also had the ability to operate with fuel injection.

The combustor was tested over a range of equivalence ratios spanning from 0.4 to 1.6 for a fixed mass flow rate of 0.045 g/s and atmospheric pressure. This resulted in a residence time of approximately 0.5 ms. For premixed hydrogen-air operation, exit gas temperatures in excess of 1800 K were achieved with combustor efficiencies of up to 70%. For non-premixed operation, peak exit gas temperatures were approximately 100 K lower with efficiencies above 65%. This reduced performance indicated that there was inadequate fuel-air mixing upstream of the combustion chamber.

Low combustor efficiencies were attributed to poor thermal isolation of the device. Chemical conversion was estimated at nearly 100% while heat transfer from the combustion chamber to the surroundings lowered the overall efficiency. The power density of the device was approximately 1200 MW/m$^3$. The device also maintained its structural integrity over tens of hours of operation. References [4] and [5] contain more detail regarding this combustor.

## 3.0 EXPERIMENTAL APPROACH

To improve upon past micro-combustor performance and to further understand the physics of these micro-scale systems, two new devices were fabricated. Both are compatible with the micro-engine design shown in Figure 1 and both combustors were constructed using the micro-fabrication techniques previously developed, as well as some new advances. The details of the design and fabrication can be found in references [5] and [8].

### 3.1 Six-Wafer Micro-Combustor

A schematic of the six-wafer micro-combustor is shown in Figure 4 alongside a scanning electron micrograph (SEM) of a cross-section of the actual device. Air, or premixed fuel-air, enters the device axially followed by a 90$^o$ turn prior to entering the compressor. For this non-rotating test device, swirl vanes were included to replicate the compressor exit flow angle of 80$^o$. The flow then passes through a duct which wraps around the combustion chamber. This passage is referred to as the *cooling jacket* and is intended to thermally isolate the combustion chamber and cool the inner walls, as well as act as a simple recuperator for preheating the reactants. This is also where fuel is injected in the non-premixed mode of operation. A set of three fuel injection ports were included to evaluate fuel-air mixing requirements.

The fuel-air mixture is then burned in the combustion chamber. Two types of chamber inlets were designed to create different flame holding recirculation zones. The first is a simple

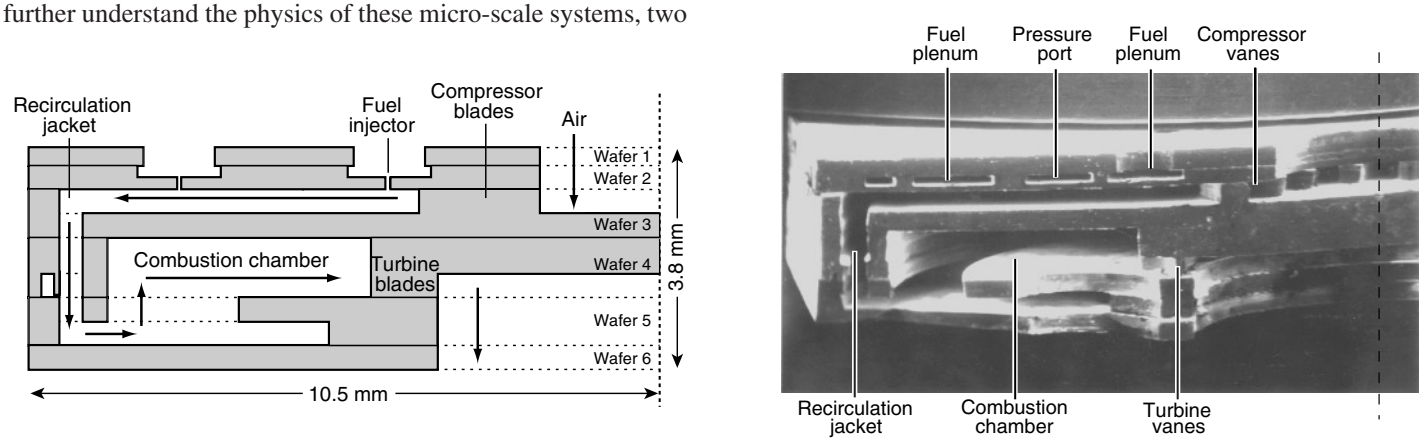


**Figure 4: Schematic and SEM of 6-wafer combustor.**

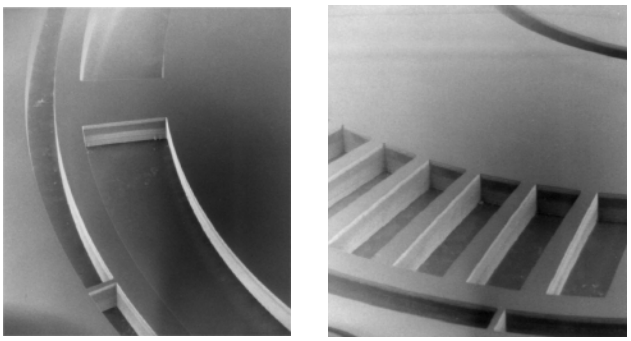

(a) (b)

**Figure 5: SEMs of combustion chamber inlets.**

annular inlet 1.2 mm wide. The second is an array of 60 slots 2.2 mm long intended to create multiple small recirculation zones for more rapid and uniform ignition of the incoming flow. SEMs of both inlets can be seen in Figure 5. Finally, the combustion products are passed through the turbine nozzle guide vanes and exit axially from the device.

### 3.2 Dual-Zone Micro-Combustor

The dual-zone micro-combustor is a modification to the six-wafer geometry, but represents a significant change in operating mode. A schematic of this device is shown in Figure 6. A series of holes through the inner wall have been created connecting the upper cooling jacket to the combustion chamber. These holes allow inlet air to bleed into the combustion chamber. This dilution air serves two purposes; first, it splits the combustion chamber into two zones, and second, it dilutes the hot combustion products reducing their temperature to the desired turbine inlet temperature of 1600 K. This is similar to conventional large-scale combustors. In the primary zone, the fuel-air mixture is burned near stoichiometric conditions. By burning at higher temperature, kinetic rates increase and reaction time decreases effectively increasing $Da_h$. The dilution jet also serves to strengthen recirculation zones and improve stability. The combustion chamber inlet for the dual-zone combustor is slotted as shown in Figure 5b. Due to the nature of this combustor's operation, premixed combustion is not feasible and fuel injection occurs just downstream of the dilution holes in the cooling jacket.

The dilution holes were designed to split the total mass flow in half, establishing a stoichiometric primary zone at the design point conditions. The overall equivalence ratio for the combustor in this case is 0.5. However, at off-design conditions, the flow split deviates from the desired 50% dilution air and the primary zone will no longer operate at $\phi = 1.0$. As mass flow rate increases, the percentage of total flow used for dilution decreases. For a fixed overall fuel/air ratio, this results in a lean primary zone.

Two variations of the dual-zone micro-combustor were fabricated to test the effect of primary zone size. These variations differed in the radial locations of dilution holes. Combustors with dilution holes located at a 5.9 mm radius and a 7.0 mm radius were constructed.

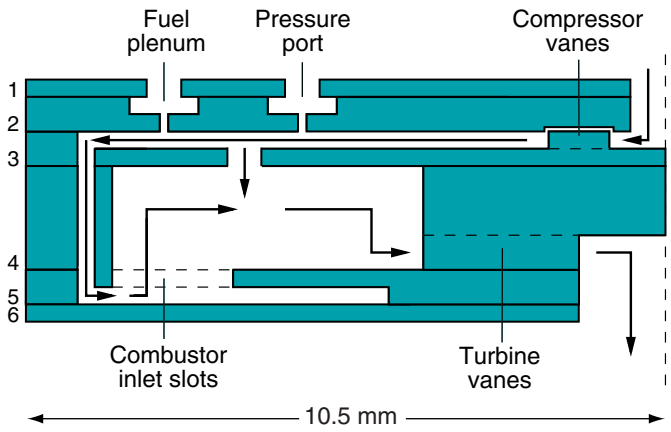


**Figure 6: Schematic of the dual-zone combustor.**

### 3.3 Experimental Setup and Diagnostics

Prior to testing, the micro-combustors were packaged into a suitable test rig. In order to connect the device's micro-scale fluid channels to a macro-scale feed system, a glass bead interconnect scheme was developed by Mehra [5]. Small kovar tubing was hermetically sealed to the silicon with glass beads and brazed to a larger invar plate for connection to conventional fittings. A fully packaged device is shown in Figure 7. A more detailed description of this process can be found in references [5, 8, 9].

Due to the micro-scale of the devices, it is difficult to obtain non-intrusive measurements. Therefore, diagnostics were limited. Exit gas temperature was measured using a 0.010 in. sheathed type K thermocouple. Because of the large temperature gradients along the length of the wire, an error analysis for the thermal conductivity, radiative emissivity, and calibration drifts predicted uncertainties up to $\pm 130$ K. A wall temperature measurement

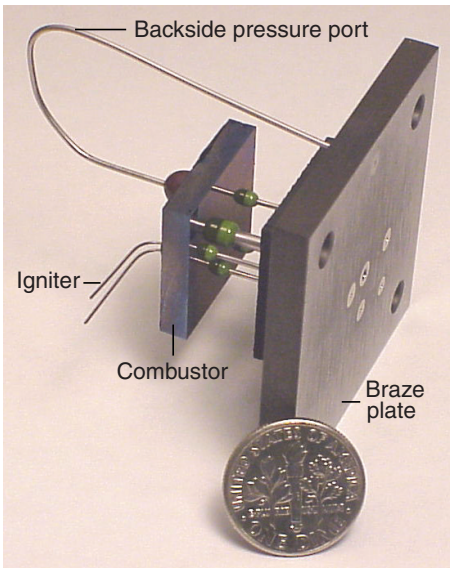


**Figure 7: Fully packaged micro-combustor.**

was also obtained with the same type thermocouple and an uncertainty of ±12 K. In addition to the temperature diagnostics, pressure was measured upstream in the cooling jacket and in the combustion chamber itself. Flow control was accomplished with several MKS Type 1359C flow controllers with ±0.5% full-scale accuracy (±0.05 SLM for air and ±0.005 SLM for fuel). A detailed uncertainty analysis can be found in reference [5].

## 4.0 RESULTS AND ANALYSIS

Overall combustor efficiency is defined as:

$$\eta_c = \frac{\left(\dot{m}_a + \dot{m}_f\right)h_2 - \dot{m}_a h_1}{\dot{m}_f h_f} \tag{6}$$

where station (1) refers to the combustor inlet and station (2) is the combustor exit. The combustor efficiency can be written as the product of two sub-efficiencies: a *chemical efficiency*, and a *thermal efficiency*. These two efficiencies can be written as:

$$\eta_{chem} = \frac{\left[\left(\dot{m}_a + \dot{m}_f\right)h_2 - \dot{m}_a h_1\right] + \dot{Q}_{loss}}{\dot{m}_f h_f} = \frac{\text{total enthalpy released}}{\text{maximum enthalpy release possible}} \tag{7a}$$

$$\eta_{therm} = \frac{(\dot{m}_a + \dot{m}_f)h_2 - \dot{m}_a h_1}{\left[(\dot{m}_a + \dot{m}_f)h_2 - \dot{m}_a h_1\right] + \dot{Q}_{loss}} = \frac{\text{enthalpy rise of fluid}}{\text{total enthalpy released}} \tag{7b}$$

### 4.1 Baseline Six-Wafer Hydrogen Tests

Baseline six-wafer micro-combustor tests were performed with premixed hydrogen-air in the annular inlet geometry. Figure 8 shows plots of combustor exit temperature and efficiency for constant equivalence ratio.

The combustor produced exit gas temperatures in excess of 1600 K for a mass flow rate of 0.11 g/s and an operating pressure of 1.13 atm. The overall efficiency in this case exceeded 90% and the power density was approximately 1100 MW/m$^3$. The break in the $\phi = 0.5$ and $\phi = 0.6$ exit temperature and efficiency curves is due to a lack of measurement capabilities for gas temperatures over 1600 K. The $\phi = 0.7$ curve terminates at a mass flow rate of 0.015 g/s due to upstream burning in the cooling jacket.

The inability of the device to achieve the design point operation of 0.36 g/s and 3 atm and the general shape of the exit temperature and efficiency curves can be explained by examining the change in $Da_h$ over a constant equivalence ratio operating line. Using the previously defined residence time and a simple one step mechanism for hydrogen-air combustion

$$\tau_{reaction} = \frac{[H_2]_0}{A[H_2]^2[O_2]e^{-E_a/RT}} \tag{8}$$

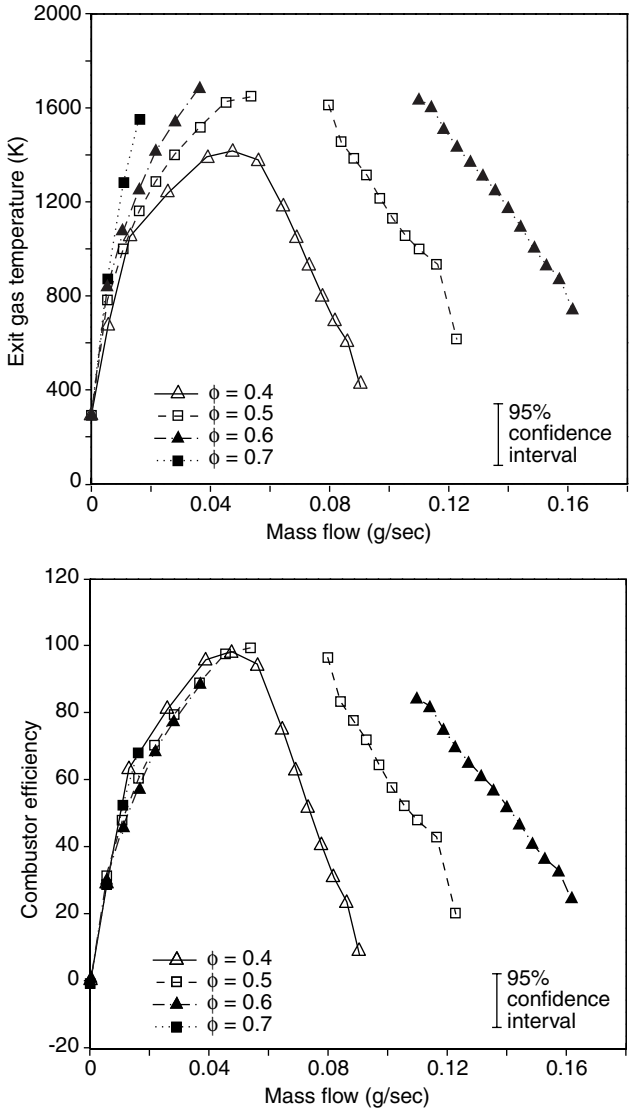


**Figure 8: Plots of exit gas temperature and efficiency for annular six-wafer combustor with premixed hydrogen-air.**

with $E_a$ = 10950 cal/mole and $A = 1.62 \times 10^{18}$, an estimate of $Da_h$ can be obtained [5]. Figure 9 shows a plot of reaction time and residence time along with $Da_h$ versus mass flow rate. Residence time decreases more rapidly than reaction time, resulting in a $Da_h$ less than one. This leads to chemical inefficiency at high mass flow rates as well as flame blow-out prior to choking the nozzle guide vanes and reaching the design point conditions.

Analysis by Mehra [5] using a 1-D heat transfer model to predict heat loss from the combustor indicates that thermal inefficiencies dominate low mass flow operation, while at high mass flows performance is limited by chemical inefficiency.

### 4.2 Comparison of Inlet Geometry

Combustor efficiency for premixed hydrogen-air tests in the

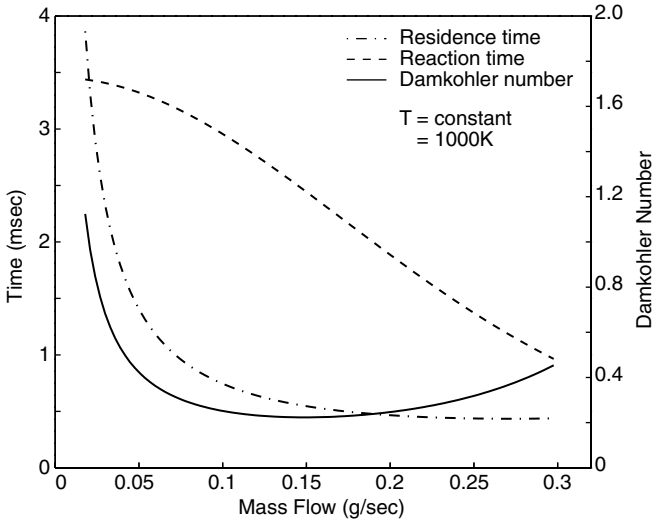


**Figure 9: Reaction time, residence time, and $Da_h$.**

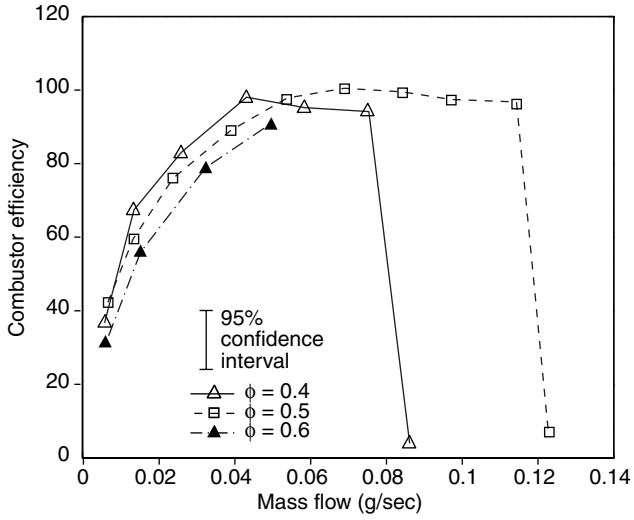


**Figure 10: Efficiency for slotted inlet six-wafer combustor.**

slotted-inlet geometry is plotted in Figure 10. Performance is similar to the annular inlet combustor, however, the slotted-inlet device produced higher exit temperatures and efficiencies in the high mass flow, kinetically limited regime of the operating line. This is attributed to the presence of multiple recirculation zones at the inlet which rapidly and uniformly ignite the incoming mixture. The sharp drop in performance for the slotted combustor is due to the rapid extinction of the ignition zones. In the annular case shown in Figure 8, the single large recirculation zone stays lit over a wider range of mass flow rates, however, it also results in lower chemical efficiency.

Numerical simulations were performed on both inlet geometries using FLUENT 5 with a nine-species, 20-step, hydrogen-air reaction mechanism for the chemical model [11]. Figure 11a shows CFD generated contours for the combustor with the annular inlet. In Figure 11b contours of temperature are plotted for a 2-D cut through the combustor inlet in the θ-z plane. These contours show a temperature gradient from the bottom of the combustion chamber to the top and indicate the primary ignition zone is in the upper right corner of the combustor. Figures 12a and 12b show the same contour plots for a combustor with a slotted inlet. The temperature contour in the θ-z plane shows significantly higher temperature in the lower regions of the combustion chamber and higher overall temperatures. The shape of the contours indicates that there are small, hot ignition zones near the slotted inlet. Additional details of the numerical simulations can be found in reference [10].

### 4.3 Fuel Injection Schemes

The performance of the three sets of fuel injectors was evaluated by comparing efficiencies with the premixed case. Pre-mixed operation consisted of fuel/air injection through the primary air inlet only. Figure 13 plots efficiency for different equivalence ratios at a mass flow rate of 0.045 g/s. The injectors

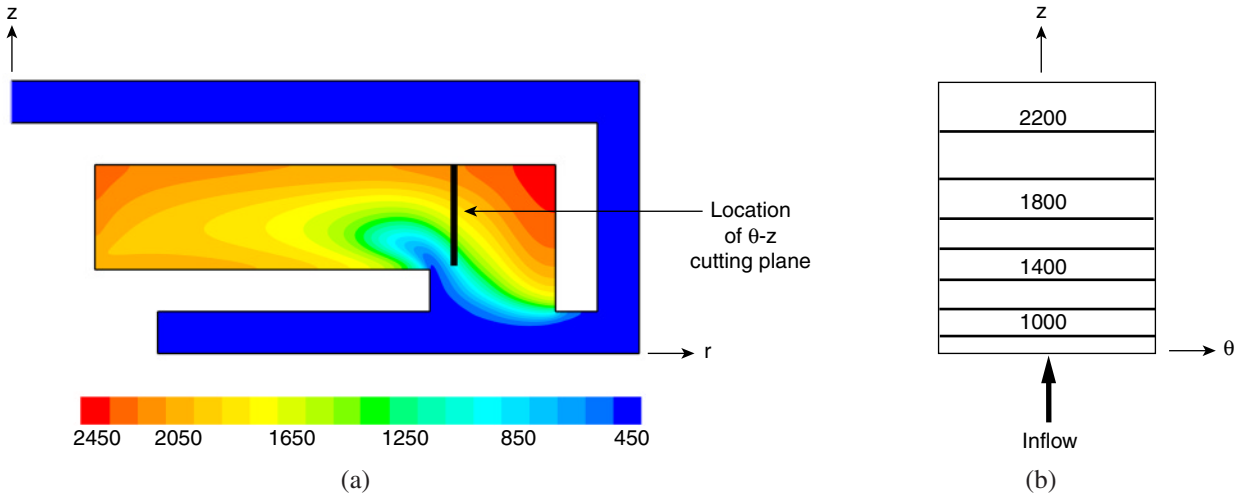


**Figure 11: Temperature (K) contours for annular inlet combustor.**

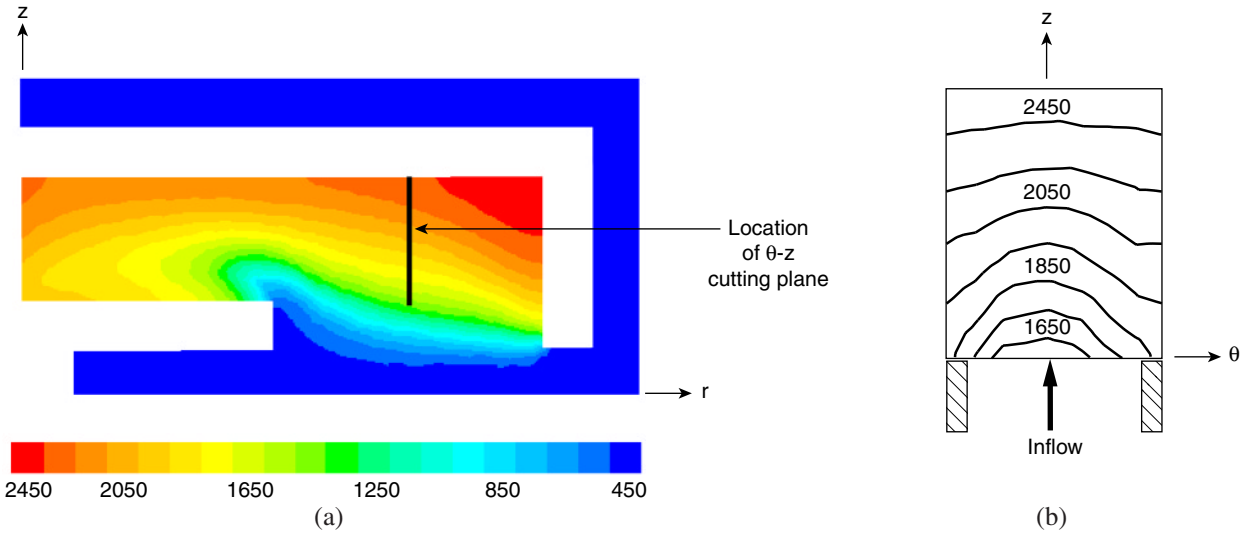


**Figure 12: Temperature (K) contours for slotted inlet combustor.**

were located at radii of 4.8 mm and 8.0 mm in the cooling jacket while a set of side-wall injectors were at the base of the cooling jacket. The figure indicates that performance decreases as the injectors get closer to the combustion chamber. This is due to the decreased mixing length.

### 4.4 Baseline Dual-Zone Hydrogen Tests

Baseline dual-zone testing was performed with hydrogen fuel injection through upstream fuel injectors at a radius of 8.0 mm. The dilution hole radial location was 7.0 mm. Plots of exit gas temperature and efficiency are shown in Figure 14. This combustor achieved exit gas temperatures in excess of 1600 K at mass flow rates exceeding 0.12 g/s and efficiencies over 85%.

The dual-zone combustor exhibited slightly lower exit gas temperature and efficiency than the single-zone, six-wafer combustor. However, its operating range was much wider. Combustion was stabilized at equivalence ratios as low as 0.2 and mass flow rates as high as 0.2 g/s. Figure 15 compares the dual-zone combustor efficiency to the single-zone for similar conditions.

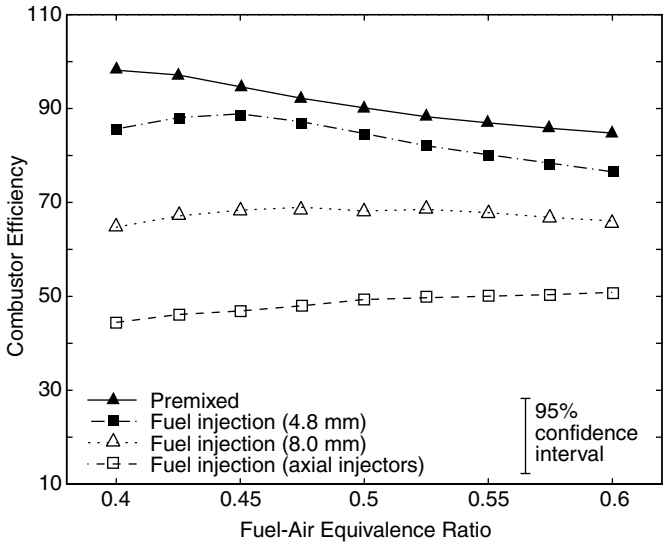


**Figure 13: Efficiency for fuel injection schemes.**

The significant extension in operating range is largely due to strengthened recirculation zones and the hot, stable primary zone. For the same overall efficiency, the dual-zone combustor achieved a 100% increase in mass flow rate before blow-out. The ability to operate at low overall equivalence ratio is a result of a higher local equivalence ratio in the primary zone. It should be noted that for the current microengine applications, combustor efficiencies of 80% or higher are acceptable.

### 4.5 Effect of Primary Zone Size

To evaluate the effects of primary zone size, dilution holes located at radii of 5.9 mm and 7.0 mm were tested. These correspond to primary zone volumes of 78.5 $mm^3$ (41% of total combustor volume) and 37 $mm^3$ (20% of total combustor volume) respectively. Figure 16 plots efficiency for the two devices operating at similar conditions. Higher mass flows were achieved with the larger primary zone. This is largely due to increased residence time in the primary zone. There was also a reduction in efficiency. This was probably due to non-uniform exit temperature profiles where the measurement was made.

### 4.6 Hydrocarbon Tests

Hydrocarbon fuels with slower reaction rates were tested in the devices. For a micro-engine to be practical, fuels such as ethylene ($C_2H_4$) and propane ($C_3H_8$) will be required due to their high energy densities and favorable storage properties. Results from combustion tests for these two fuels in the six-wafer combustor are shown in Figure 17. The ethylene-air mixture achieved maximum power density at an equivalence ratio of 0.9 and 1 atm pressure, with exit temperature exceeding 1400 K and efficiency of 60%. The estimated power density for these

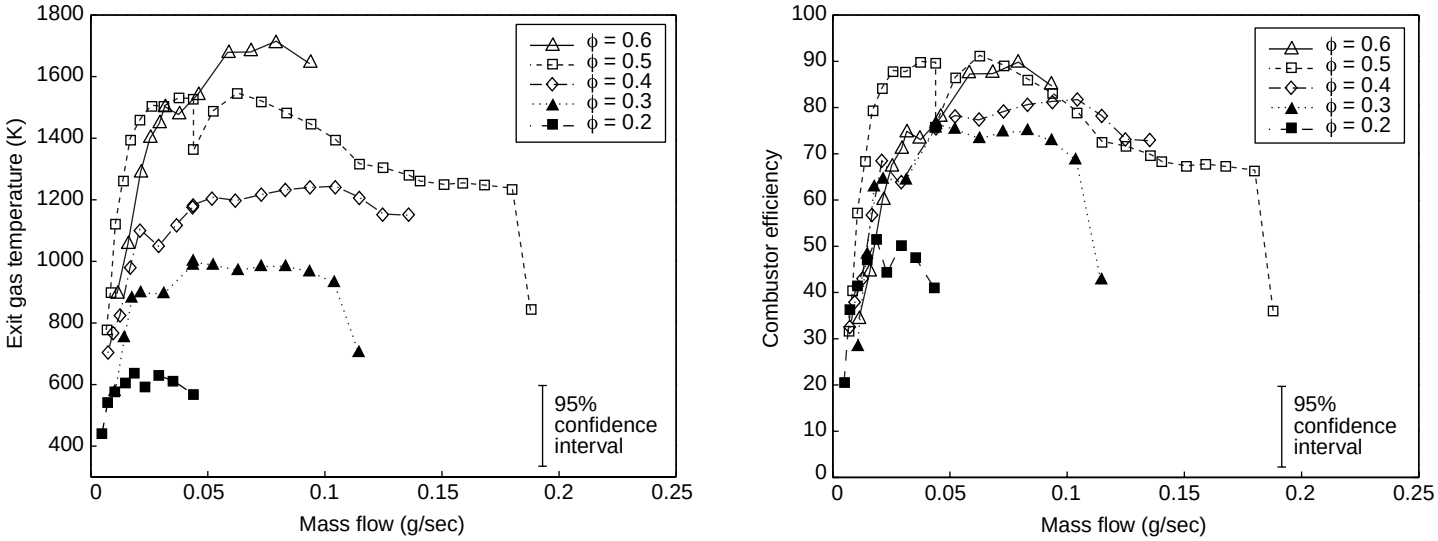


**Figure 14: Plots of exit gas temperature and efficiency for dual-zone combustor with hydrogen-air.**

conditions is ~500 MW/m$^3$. The reaction rates of propane are significantly lower than ethylene and as a result, combustion could only be stabilized in the device at an equivalence ratio of 0.8. Exit temperatures of 1200 K were reached at 1 atm with an efficiency of 55%. This corresponds to a power density of ~140 MW/m$^3$. Nominal residence times for ethylene-air and propane-air combustion in this device were 1.6 ms and 2.8 ms respectively. Typical reaction times are 0.5-1 ms for ethylene-air and 1-2 ms for propane-air whereas hydrogen-air reaction times are approximately 0.2 ms.

The dual-zone combustor did not provide an expected broader range of mass flow for hydrocarbon-fueled operation. This is believed to be due primarily to inadequate mixing lengths, since the fuel injectors were designed for operation with hydrogen. As a result, mass flows of only up to 0.06 g/s and efficiencies less than 50% were achieved with ethylene. However, these combustors were operated with a wider range of equivalence ratios. This was due in part to fuel injection, which prevented upstream burning and allowed higher mixture ratios. In addition, lower equivalence ratios were possible due to the strengthened recirculation zones created by the dilution flow. Figure 18 shows efficiency for both ethylene-air and propane-air combustion in a dual-zone combustor with dilution holes located 7.0 mm radially outward. The maximum power density achieved for the ethylene-air mixture was ~100 MW/m$^3$ and 75 MW/m$^3$ for propane-air with residence times of 2.1 ms and 3.7 ms respectively.

## 5.0 OPERATING SPACE

Figure 19 plots the empirically identified operating space for the baseline six-wafer and the dual-zone micro-combustors

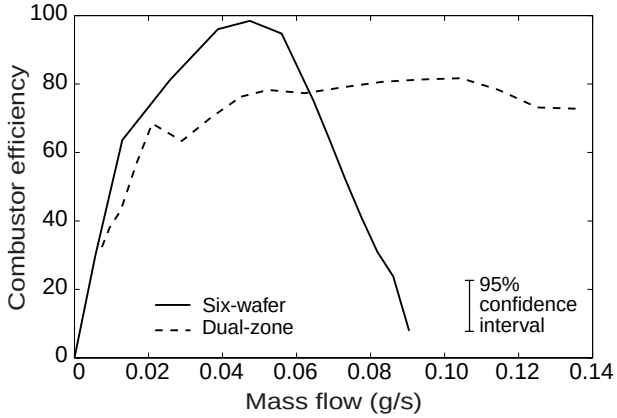


**Figure 15: Efficiency comparison of dual-zone combustor to baseline six-wafer combustor.**

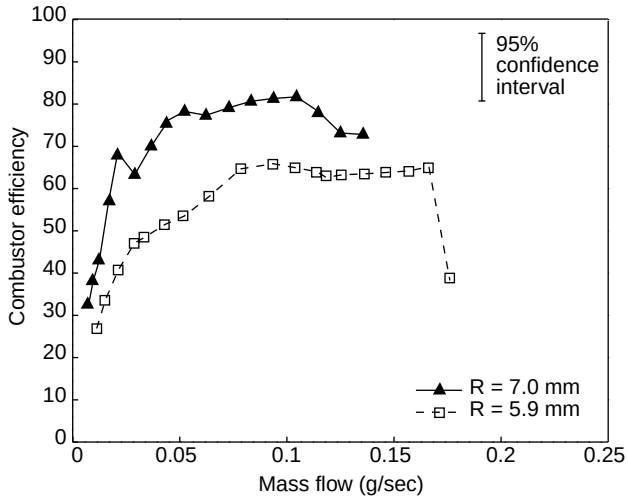


**Figure 16: Comparison of dual-zone combustors with different primary zone sizes.**

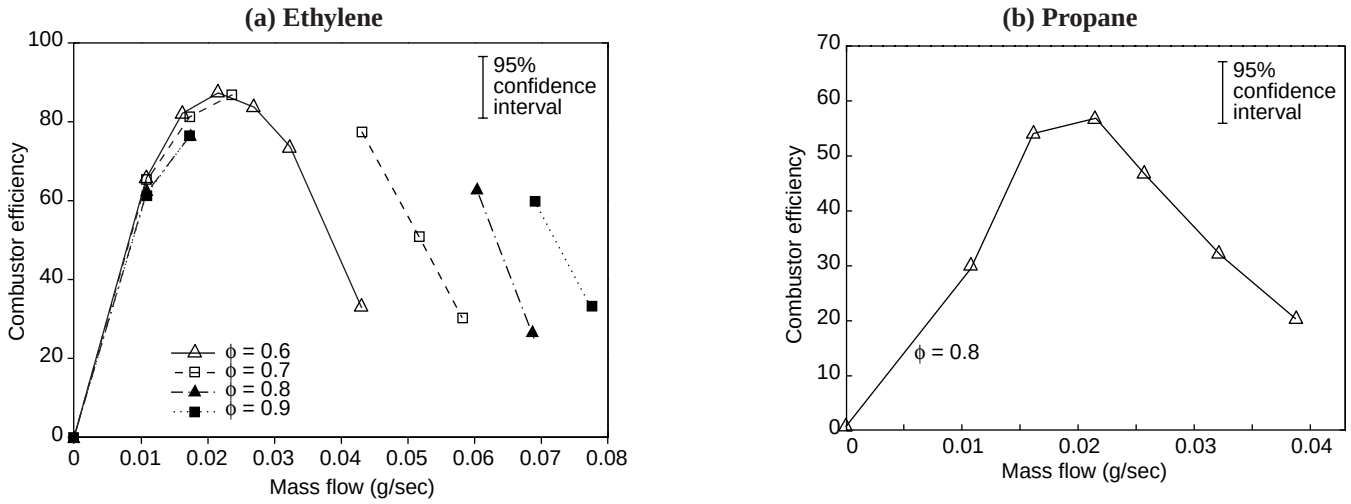


**Figure 17: Efficiency for ethylene and propane in the baseline six-wafer combustor.**

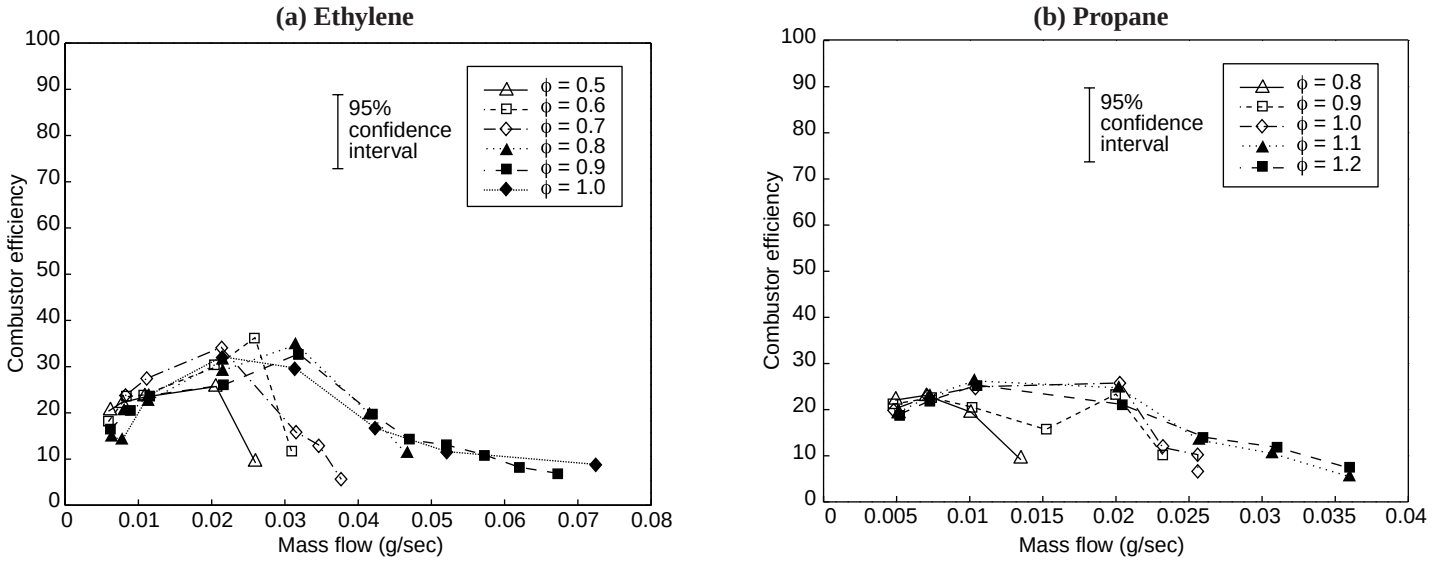


**Figure 18: Efficiency for ethylene and propane in the dual-zone combustor.**

burning hydrogen. The operating boundaries include:

1. The lean blow-out limit.
2. The upstream burning limit where combustion in the cooling jacket occurred.
3. The structural limit.
4. The 1600 K $T_{t4}$ micro-engine cycle limit (assuming 80% combustor efficiency).

A narrow operating corridor exists between the lean blow-out limit and the upstream burning limit, however, as previously discussed, the design mass flow rate of 0.36 g/s was not reached. As a result, initial engine designs will have reduced flow (225 μm compressor blade height instead of 400 μm blade height).

The dual-zone combustor has a broader operating space due to the stable, hot primary zone. The most notable features of this operating space are: the lower lean blow-out limit and the absence of an upstream burning limit due to non-premixed operation.

Figure 20 shows data for all of the combustors, including the three-wafer device mentioned in section 2.6, presented in a plot of Damköhler number versus chemical efficiency. The wall temperature measurements along with a simple 1-D heat transfer model were used to estimate the heat loss from the devices enabling a calculation of chemical efficiency [5]. The residence time was calculated using the exit gas temperature measurements while Chemkin III, a reaction kinetics software package, was used to compute chemical time-scales. The nine species, 20 step hydrogen-air reaction mechanism used for the CFD simulations was utilized as the chemical model [11]. For hydrocarbon-air cases GRIMech 3.0 was used. As Damköhler number increases, chemical efficiency asymptotically approaches unity. Points to

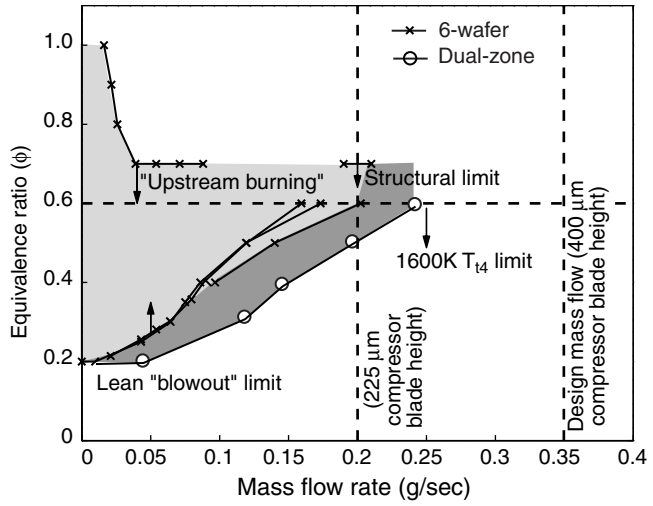


**Figure 19: Operating space for six-wafer and dual-zone combustors.**

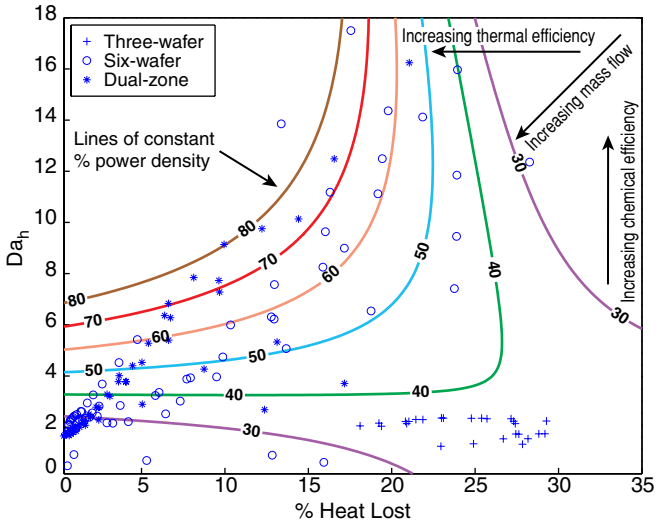


**Figure 21: Non-dimensional operating space.**

the far left with low chemical efficiency are a result of the combustor approaching blow-out in the high mass flow regions of the operating space.

Although Figure 20 shows high chemical efficiency over a range of Damköhler numbers, the performance of these devices was found to be a function of both chemical and thermal losses. In this case performance is quantified in terms of non-dimensional power density, or actual power density normalized by the maximum possible power density at those conditions.

If it is assumed that there is adequate fuel-air mixing and rapid, uniform ignition, this parameter is a function of only two parameters; Damköhler number and non-dimensional heat loss. Damköhler number was estimated as previously described using exit gas temperature measurements for residence time

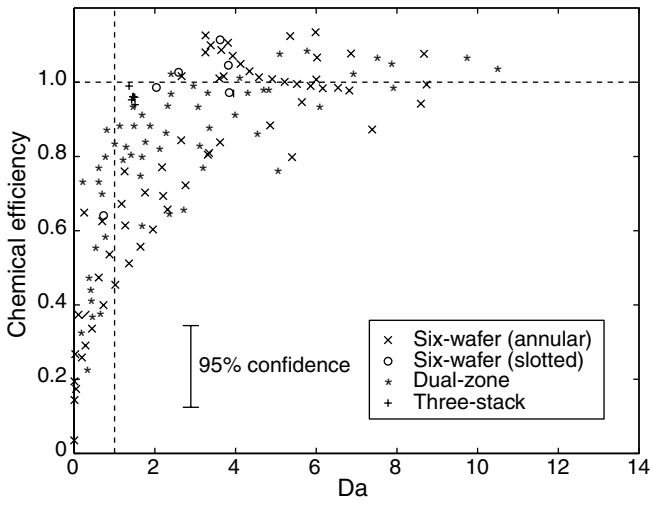


**Figure 20: Damköhler number vs. chemical efficiency for several micro-combustors.**

calculations and Chemkin III for chemical time approximations. Heat loss can be cast in non-dimensional terms by normalizing the actual heat lost from the device by the maximum possible heat which can be generated at a given operating condition. Again, the actual heat lost was estimated using a 1-D heat transfer model [5].

Figure 21 plots this non-dimensional power density for all of the combustors in three-parameter space. The plot includes all three fuels tested (hydrogen, ethylene and propane). The heat loss parameter and Damköhler number are on the x and y-axes, respectively. A second order, least squares surface fit was used to generate contours of non-dimensional power density (the fit explains 62% of the variance in the data).

Thermal efficiency in these devices is inversely proportional to heat loss while chemical efficiency is directly proportional to Damköhler number. Hence, optimum performance is achieved at low levels of heat loss and high Damköhler number as indicated in Figure 21.

This non-dimensional operating space further explains the operating line considerations of a micro-combustor. Conditions of increasing mass flow for constant equivalence ratio move from the upper right side of the operating space to the lower left. In the low mass flow region of the space, performance is limited by heat loss, while at high mass flow Damköhler number falls and performance is limited by chemical inefficiency. In the area of moderate mass flow, the center of the operating space, the highest power densities are achieved. This is consistent with the data presented in section 4 where the highest overall efficiencies were found to be at moderate mass flow rates. Although we do not present the results here, the overall trends shown in Figure 21 are consistent with what has been obtained from a PSR model with heat loss run for the same operating space.

Figure 21 also indicates that the micro-combustor design changes discussed previously improved overall performance.

The three-wafer combustor suffered from high heat loss and lies to the lower right in the operating space. The largest performance enhancement came with the implementation of the cooling jacket for thermal isolation of the combustion chamber. The six-wafer data lies much farther to the left (low heat loss region) and also has higher Damköhler numbers. The dual-zone combustors provided a hot stable flame-zone which resulted in higher Damköhler numbers and improved performance.

This non-dimensional operating space can also be useful in the design process. For example, a good estimate of the volume required for a propane-air micro-combustor suitable for a micro gas turbine can be obtained. If similar conditions to those run here are assumed (1600 K exit gas temperature, 1 atm pressure, and mass flow of 0.15 g/s) and an equivalence ratio of $\phi = 0.8$ is selected, the non-dimensional power density can be computed and is approximately 60%. The heat loss from the device can be assumed to be approximately 5% based on previous data with thermal management techniques such as the cooling jacket. From Figure 21, the desired Damköhler number can be found and is approximately 5.5. The chemical time can be computed using Chemkin III or any other suitable technique and the desired residence time found from the Damköhler number. This results in a residence time of 1.44 ms and a volume of 950 $mm^3$, or about a fivefold increase in volume compared to those combustors presented here.

## 6.0 DESIGN RECOMMENDATIONS

The following design trades and recommendations for micro-combustion systems have been identified:

1. The high power density requirements of a micro-combustor mandate high mass flow rates per unit volume. However, this results in low residence time and Damköhler numbers of order unity. Micro-combustion systems are fundamentally limited by this trade-off between high power density and efficient combustion.
2. The large surface-area-to-volume ratio of a micro-combustor makes non-adiabatic operation intrinsic to its design. The coupling between heat transfer and chemical kinetics is a critical element of the design process. Thermal isolation of the device improves thermal efficiency, however, cold walls are detrimental to reaction rates. Strategies such as the cooling jacket presented here are effective solutions. While keeping the inner wall cool, it acts as a fuel-air pre-heater to improve kinetic rates, offsetting the effect of lower wall temperatures.
3. Recirculation zones are critical for rapid and uniform ignition of incoming reactants. However, if these ignition zones are too large, the effective volume of the combustion chamber will be significantly reduced resulting in decreased residence time and $Da_h$. Flame holding ignition zones should be carefully tailored to balance these two effects.
4. Fuel injection for non-premixed operation should occur as far upstream of the combustion chamber as possible to provide adequate mixing length.
5. It is not sufficient to design a micro-combustor exclusively for design point operation. Operating line issues need to be considered. For the combustors presented here, the minimum $Da_h$ occurs at mass flows and pressures corresponding to operation prior to choking of the nozzle guide vanes.

## 7.0 SUMMARY AND CONCLUSIONS

Although micro-scale combustion systems have similar functional requirements to conventional combustors, residence time and heat transfer effects significantly impact the design. To explore these phenomena at the micro-scale, two devices were fabricated and tested while numerical simulations were also conducted.

The test devices consisted of six silicon wafer levels and a combustion chamber measuring 191 $mm^3$. Premixed hydrogen-air combustion was sustained at exit temperatures greater than 1600 K, efficiencies over 90%, and power densities up to 1100 $MW/m^3$. Non-premixed hydrogen-air combustion was stabilized with similar performance. Hydrocarbon fuels were also burned in the devices and achieved efficiencies of up to 60% and power densities near 500 $MW/m^3$. It was found that the low mass flow regime of the operating space was limited by thermal losses, while in the high mass flow regime, chemical inefficiency dominated. Multiple fuel injection schemes and inlet geometries were tested. The importance of recirculation zones to rapidly and uniformly ignite reactants was identified and supported by numerical simulations and analysis. The operating space for these combustors was mapped and additional boundaries such as upstream burning were noted. The broadening of this space by the implementation of a hot primary zone and dilution region was observed. A non-dimensional operating space was developed and shown to be useful as a design tool.

Experimental and computational work is continuing with a focus on a hydrocarbon-fueled micro-combustor. Alternate combustion strategies are being investigated and a catalytic hydrocarbon combustor is in development.

## 8.0 ACKNOWLEDGMENTS

This work was conducted as part of the MIT Microengine Project supervised by Professor Alan Epstein. The authors are grateful to Professor Epstein for his direction throughout the course of this research and also to Professor Martin Schmidt of the MIT Microsystems Technology Laboratory and Dr. A Ayon. We also acknowledge the technical support of Greg Simpson at Thunderline-Z Inc. and the Gas Turbine Laboratory technical staff; Viktor Dubrowski, James LeTendre, and William Ames. The administrative support of Lori Martinez and Holly Anderson, as well as the editorial assitance of Diana Park, is also greatly appreciated. The authors also thank the entire microengine team especially Dr. Eugene Huang, Dr. Chris Cadou, Jhongwoo Peck, and Khoon Tee Tan. All devices were fabricated at the MIT Microsystems Technology Laboratory; the assistance of the technical staff is also acknowledged. This work has been sponsored by the Army Research Office (DAAG55-98-1-0292) under Dr. T. Doligalski and by DAPRA (DAAG55-98-1-0365,

DABT63-98-C-0004) under Dr. R. Nowack and Dr. R. Rosenfeld, respectively.

## REFERENCES

[1] Epstein *et al*., "Micro-Heat Engines, Gas Turbines, and Rocket Engines", presented at the 28th AIAA Fluid Dynamics Conference, 1997.

[2] Groshenry, C., "Preliminary Study of a Micro-Gas Turbine Engine", S.M. Thesis, Massachusetts Institute of Technology, 1995.

[3] Waitz, I.A., Gautam, G., Tzeng, Y-S, "Combustors for Micro Gas Turbine Engines", *ASME Journal of Fluids Engineering*, Vol. 20, pp. 109-117, March 1998.

[4] Mehra, A., Waitz, I.A., "Development of a Hydrogen Combustor for a Microfabricated Gas Turbine Engine", presented at the Solid-State Sensor and Actuator Workshop at Hilton Head, 1998.

[5] Mehra, A., "Development of a High Power Density Combustion System for a Silicon Micro Gas Turbine Engine", Ph.D. Thesis, Massachusetts Institute of Technology, 2000.

[6] Dodds *et al*., "Combustion System Design", *Design of Modern Gas Turbine Combustors*, Mellor, A. M. (Editor), Academic Press Limited, 1990.

[7] Ballal *et al*., "Weak Extinction Limits of Turbulent Flowing Mixtures", *ASME Journal of Engineering for Power*, Vol. 101, No. 3, 1979.

[8] Mehra *et al*., "A 6-Wafer Combustion System for a Silicon Micro Gas Turbine Engine", *IEEE/ASME Journal of Microelectromechanical Systems*, 2000.

[9] Harrison, T., "Packaging of the MIT Microengine", S.M. Thesis, Massachusetts Institute of Technology, 2000.

[10] Lee, J., "Numerical Simulation of a Hydrogen Microcombustor", S.M. Thesis, Massachusetts Institute of Technology, 2000.

[11] Yetter, R.A., Dryer, F.L., Rabitz, H., "A Comprehensive Reaction Mechanism for Carbon Monoxide/Hydrogen/Oxygen Kinetics", *Combustion Science and Technology*, Vol. 79, pp. 97-128, 1991.